DRUG DELIVERY
2021, VOL. 28, NO. 1, 478–486
https://doi.org/10.1080/10717544.2021.1889717

Taylor & Francis
Taylor & Francis Group

RESEARCH ARTICLE

OPEN ACCESS Check for updates

Topical anesthetic and pain relief using penetration enhancer and transcriptional transactivator peptide multi-decorated nanostructured lipid carriers

Tao Jiang, Shuangshuang Ma, Yangyang Shen, Yuwen Li, Ruirui Pan and Huaixin Xing

Department of Anesthesiology, Shandong Cancer Hospital and Institute, Shandong First Medical University and Shandong Academy of Medical Sciences, Jinan, China

ABSTRACT

Many strategies have been developed to overcome the stratum corneum (SC) barrier, including functionalized nanostructures. Chemical penetration enhancers (CPEs) and cell-penetrating peptides (CPP) were applied to decorate nanostructured lipid carriers (NLC) for topical anesthetic and pain relief. A novel pyrenebutyrate (PB-PEG-DSPE) compound was synthesized by the amide action of the carboxylic acid group of PB with the amido groups of DSPE-PEG. PB-PEG-DSPE has a hydrophobic group, hydrophilic group, and lipid group. The lipid group can be inserted into NLC to form PB functional NLC. In order to improve the penetrability, TAT and PB multi-decorated NLC were designed for the delivery of lidocaine hydrochloride (LID) (TAT/PB LID NLC). The therapeutic effects of NLC in terms of *in vitro* skin penetration and *in vivo* in animal models were further studied. The size of TAT/PB LID NLC tested by DLS was 153.6 ± 4.3 nm. However, the size of undecorated LID NLC was 115.3 ± 3.6 nm. The PDI values of NLC vary from 0.13 ± 0.01 to 0.16 ± 0.03. Zeta potentials of NLC were negative, between −20.7 and −29.3 mV. TAT/PB LID NLC (851.2 ± 25.3 μg/cm^2) showed remarkably better percutaneous penetration ability than PB LID NLC (610.7 ± 22.1 μg/cm^2), TAT LID NLC (551.9 ± 21.8 μg/cm^2) ($p < .05$) and non-modified LID NLC (428.2 ± 21.4 μg/cm^2). TAT/PB LID NLC exhibited the most prominent anesthetic effect than single ligand decorated or undecorated LID NLC *in vivo*. The resulting TAT/PB LID NLC exhibited good skin penetration and anesthetic efficiency, which could be applied as a promising anesthesia system.

ARTICLE HISTORY
Received 30 October 2020
Revised 3 February 2021
Accepted 9 February 2021

KEYWORDS
Local anesthetics; topical anesthetics; chemical penetration enhancers; transcriptional transactivator peptide; nanostructured lipid carriers

1. Introduction

Transdermal drug delivery systems (TDDS) have been interesting research topics in the field of local anesthetics, namely topical anesthetics, because of their advantages including their painless properties, improved patient compliance, without hepatic first-pass effect, etc (de Araújo et al., 2013; Wang et al., 2013, 2016). However, there still exist obstacles to the clinical application of topical anesthetics. The stratum corneum (SC), the most out-layer of the skin epidermis, is the main permeability barrier to the transport of drugs through the skin (Mueller et al., 2016; Münch et al., 2017). Many strategies have been developed to overcome the stratum corneum (SC) barrier, including chemosmosis enhancers, nanostructures, and functionalized nanostructures (Pham et al., 2016; Gul et al., 2018).

Chemical penetration enhancers (CPEs) have widely used in transdermal drug delivery systems to aid dermal absorption of curatives and esthetics (Williams & Barry, 2004; Karande et al., 2005). CPEs can be classified into several classes: surfactants, fatty acids, fatty esters, azones, and pyrenebutyrate (PB) (Karande et al., 2004; Ookubo et al., 2014). These compounds are very different in regard to their chemical and physical properties and act in different ways to influence the SC for promoting absorption (Pino et al., 2014). Researchers have reported that triterpene saponin glycosides as CPEs enhanced the transdermal transport of water-soluble anesthetics at low concentrations (Mathew & Kuriakose, 2013). Ookubo et al have combined pyrebutyrate with a cell-membrane-permeable peptide as a transdermal delivery system (Candan et al., 2012). (1-pyrenyl)butyric acid (pyrenebutyrate, PB) was attracting interest because of its functionalized property or improving permeation, such as PB functionalized chitosan matrix, PB and cell-penetrating peptides combined application (Candan et al., 2012; Mathew & Kuriakose, 2013). The negative charge and hydrophobicity of PB could affect the migration translocation action of cell-penetrating peptides in the skin (Takeuchi et al., 2006). It is thought that their combination is beneficial to the transdermal transport of hydrophilic chemicals (Ookubo et al., 2014).

Cell-penetrating peptides (CPP) consist of a great amount of basic arginine (poly-arginine) or amino acids lysine. There are many advantages in the application of CPP: enhanced

CONTACT Huaixin Xing huaixinxingsdpc@163.com Department of Anesthesiology, Shandong Cancer Hospital and Institute, Shandong First Medical University and Shandong Academy of Medical Sciences, 440, Jiyan Road, Jinan 250117, China

skin permeability, bioadhesion, biocompatibility, biodegradable, safe passage, and transdermal delivery of drugs (Patlolla et al., 2010; Kumar et al., 2015). Recently, more and more interest has been focused on the utilization of transcriptional transactivator peptide (TAT, one of CPPs), in topical or transdermal drug delivery (Nasrollahi et al., 2012). Researchers have designed TAT decorated nanoparticles for the topical delivery of local anesthetics (Wang et al., 2013, 2016; Chen & You, 2017). Functionalization of nanoparticles with TAT further enhances their potential for achieving unattainable local anesthesia effects.

Nanoparticles (NPs) utilized for TDDS include polymeric NPs, liposomes, solid lipid nanoparticles (SLN), and nanostructured lipid carriers (NLC) (Franz-Montan et al., 2017). NLC, as the second generation of SLN, consist of a mixture of solid and liquid lipids (Müller et al., 2011). The inner matrix of NLC decides its advantages over SLN such as more drug loading and physicochemical stability. NLC has been successfully used for targeting drugs by TDDS. In the field of topical anesthesia, the most desirable marketed formulation is the eutectic mixture of lidocaine and prilocaine (EMLA® Cream, AstraZeneca). However, its clinical application is limited because of the low anesthesia pain effect (Franz-Montan et al., 2008). Therefore, we designed multi-functionalized NLC to expect to achieve some breakthrough progress.

In this paper, we synthesized a novel PB (PB-PEG-DSPE) compound by the amide action of the carboxylic acid group of PB with the amido groups of DSPE-PEG. PB-PEG-DSPE has a hydrophobic group, hydrophilic group, and lipid group. The lipid group can be inserted into NLC to form PB functional NLC. In order to improve the penetrability, TAT and PB multi-decorated NLC were designed for lidocaine hydrochloride (LID) delivery.

2. Materials and methods

2.1. Materials

1-Ethyl-3(3-dimethylaminopropyl)carbodiimide (EDC), Nhydroxysuccinimide (NHS), dimethylformamide (DMF) were provided by Aladdin Reagent Database Inc (Shanghai, China). Miglyol® 812 was purchased from Caelo (Hilden, Germany). Compritol® 888 ATO (ATO) and glycerol monostearate (GMS) were obtained from Gattefossé (Saint-Priest, Lyon, France). Injectable soya lecithin (ISL) was purchased from Lipoid GmbH (Ludwigshafen, Germany). lidocaine (LID), and Pluronic 68 (P68) were purchased from Sigma-Aldrich (St Louis, MO). TAT-PEG-DSPE was obtained from Xi'an Ruixi Biological Co., Ltd (Xi'an, China) Dulbecco's modified Eagle's medium (DMEM), fetal bovine serum (FBS), and 3-(4,5-dimethyl-2-thiazolyl)-2,5-diphenyl-2-H-tetrazolium bromide (MTT) were purchased from Invitrogen Corporation (Carlsbad, CA). L929 cell line from mouse (L929 cells) was procured from the American Type Culture Collection (Manassas, VA) and cultured in DMEM + 2 mM Glutamine + 10% Fetal Bovine Serum (FBS) medium. Kunming mice (6 to 8-weeks-old) and Wistar rats (9 to 11-weeks-old) were procured from Beijing Vital River Laboratory Animal Technology Co., Ltd. (Beijing, China), and animal handling methods got permission from the Medical Ethics Committee of Shandong Cancer Hospital and Institute.

2.2. Synthesis of PB-PEG-DSPE

PB-PEG-DSPE was synthesized by forming a conjugating amide linkage between PB and DSPE-PEG (Figure 1) (Song et al., 2018). Briefly, EDC (1.5 mmol) and NHS (1.5 mmol) were added at 0 °C to activate the carboxylic acid groups of PB (1 mmol) in DMF (10 mL, 1 h). Then PEG-DSPE (1 mmol) was dissolved in DMF (10 mL) and added dropwise to PB solution. The reaction was preceded by stirring (room temperature, 24 h), then and dialyzed (MWCO 3.5 kDa) against the deionized water for 48 h. PB-PEG-DSPE was freeze-dried and placed at 4 °C until use. PB-PEG-DSPE was analyzed by ^{1}H-NMR spectroscopy.

2.3. Preparation of NLC

Solvent diffusion technology was used to prepare LID loaded NLC (LID NLC) (You et al., 2017). Oil phase: After mixing GMS (100 mg), ATO (100 mg), and Miglyol® 812 (100 mg) and heating to 80 ± 2 °C, the oil phase was obtained; DMF (3 mL) was used to dissolve LID (50 mg), PEG-DSPE (200 mg), and ISL (50 mg) and mixed with the oil phase. Simultaneously, Pluronic 68 (P68) was dispersed in Milli-Q water (50 mL) to form an aqueous solution. The aqueous phase was stirred at the speed of 600 rpm and then we injected the oil phase rapidly into it. LID NLC was obtained through dialysis the mixture with PBS (pH 7.4) for 6 h. Single TAT or PB decorated, LID loaded NLC (TAT LID NLC or PB LID NLC) were produced by the same method using PB-PEG-DSPE (200 mg) or TAT-PEG-DSPE (200 mg) instead of PEG-DSPE (200 mg). TAT and PB multi-decorated, LID loaded NLC (TAT/PB LID NLC, Figure 2) was produced by a similar procedure using PB-PEG-DSPE (100 mg) plus TAT-PEG-DSPE (100 mg) instead of PEG-DSPE (200 mg). Blank TAT and PB multi-decorated NLC (TAT/PB NLC) were produced by the same method without adding LID.

2.4. Morphology, size, and zeta potential of NLC

Morphology and size of TAT/PB LID NLC were visualized by a Transmission Electron Microscope (JEOL 1400, Tokyo, Japan) (Mandal et al., 2016). The diluted samples were dropped into the copper mesh, and the sodium silicotungstate (1%, w/v) was negatively stained. Dynamic light scattering (DLS) technique was used to measure the average particle size, polydispersity index (PDI), and zeta potential of NLC at room temperature on Malvern ZetaSizer Nano ZS90 (Malvern Instruments Ltd, Malvern, UK).

2.5. Drug encapsulation efficiency and loading content

A gel filtration method was applied to evaluate drug encapsulation efficiency (EE) and loading content (DL) of LID-loaded NLC (Wang et al., 2016). LID was separated from the NLCs Sephadex G50 column (GE Healthcare Bio-Sciences,

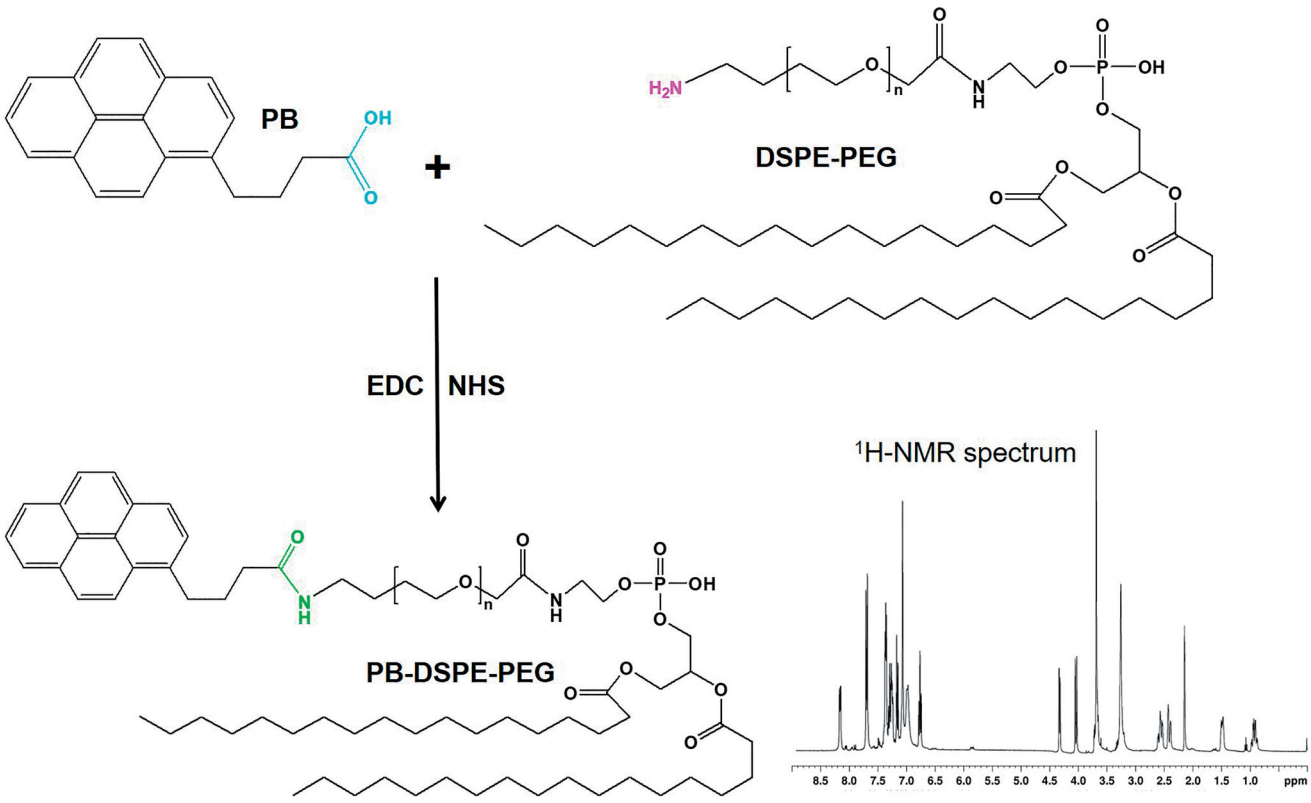

Figure 1. Synthesis of PB-PEG-DSPE. PB-PEG-DSPE was synthesized by conjugating PB with the amido groups of DSPE-PEG through amide formation.

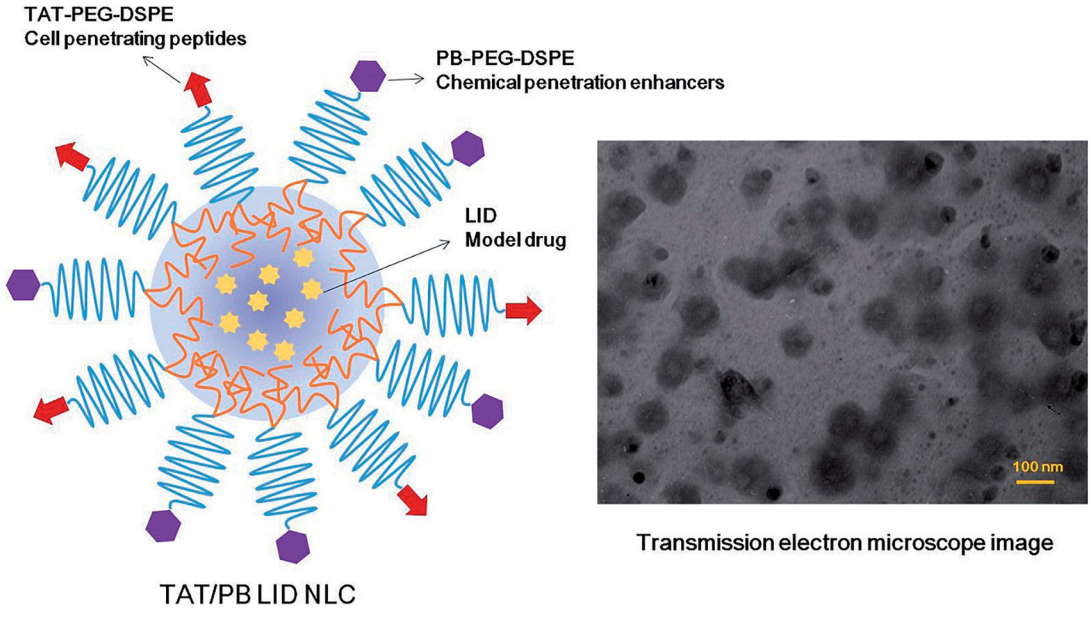

Figure 2. Scheme graph and transmission electron microscope image of TAT/PB LID NLC. TAT/PB LID NLC was prepared by solvent diffusion method. The morphology and size of TAT/PB LID NLC was visualized by a transmission electron microscope.

Pittsburgh, PA) and HPLC was utilized to determine the content of LID. A zorbax RP-select B column (Agilent Technologies, Santa Clara, CA) was used and 0.01 M sodium dihydrogen phosphate–methanol (25:75, v/v) was prepared as the mobile phase with a determined flow rate (1 mL/min). A wavelength of 260 nm was performed to calculate the EE and DL by formulations (1) and (2):

$$\text{EE}\ (\%) = \frac{(\text{The amount of total drug} - \text{The amount of free drug})}{(\text{The amount of total drug})} \times 100. \quad (1)$$

$$\text{DL}\ (\%) = \frac{(\text{The amount of total drug} - \text{The amount of free drug})}{(\text{The amount of total lipid})} \times 100. \quad (2)$$

Table 1. Characterization of NLC.

Formulation	Particle size (nm)	PDI	Zeta potential (mV)	EE (%)	DL (%)
LID NLC	115.3 ± 3.6	0.13 ± 0.01	−29.3 ± 2.6	91.6 ± 2.8	12.3 ± 1.5
TAT LID NLC	152.7 ± 4.8	0.16 ± 0.02	−21.2 ± 1.9	90.1 ± 3.1	9.4 ± 0.9
PB LID NLC	141.1 ± 3.9	0.14 ± 0.02	−27.6 ± 2.9	89.5 ± 2.9	8.9 ± 0.7
TAT/PB LID NLC	153.6 ± 4.3	0.15 ± 0.03	−20.7 ± 2.3	88.7 ± 3.3	8.1 ± 0.8
TAT/PB NLC	154.1 ± 4.7	0.16 ± 0.03	−22.4 ± 2.5		

Data represents the mean ± SD, $n = 3$.

2.6. Storage stability of NLC

To evaluate the storage stability of NLC at 2–8 °C, the mean particle size, PDI, EE and DL were tested at 0, 10, 20, 30, 60, 90 days during 3 months (Yue et al., 2018).

2.7. In vitro drug release of NLC

The dialysis method was applied to evaluate the *in vitro* drug release of LID from the NLC (Zhao et al., 2018). Briefly, NLC formulations (1 mL each) were sealed into a semi-permeable dialysis membrane (molecular weight cut off of 50 KDa), respectively. Semi-permeable dialysis bags (molecular weight cut off of 50 KDa) were used to fill with NLC formulations (1 mL each) and immersed in the phosphate-buffered saline (PBS, pH 7.4). After shacking at 100 rpm (37 °C), samples (0.5 mL) were collected from the release media at determined time points (1, 2, 4, 8, 16, 24, 36, 48, and 72 h) and replaced with fresh PBS (0.5 mL) to keep the sink condition. The released LID was analyzed using the method presented in Section 2.5.

2.8. In vitro percutaneous penetration effect of NLC

The mice were dislocated and killed. The rat's abdomen was carefully shaved with an electric razor to avoid damaging the cuticle. Remove the skin from the abdominal surface and remove the attached fat and subcutaneous tissue (Wang et al., 2013). Vertical Franz-type diffusion cells (volume 7.0 mL, ross-sectional area 5.93 cm^2) were used (Yue et al., 2018). The skin was strapped to the donor chamber with the dorsal side facing upwards. The receptor compartment was filled with 0.9% saline (7.0 mL) containing anhydrous ethanol (2%, w/w) at 37 °C, and the solution was continuously stirred at a speed of 300 rpm. LID loaded NLC and free LID (0.5 mL, concentration of LID was 2 mg/mL) were placed on the skin. Samples (0.3 mL) were collected in the receptor phase at determined time points (1, 2, 4, 8, 12, 16, 24, 36, 48, and 72 h) and the same volume of PBS was added. The permeated LID was extracted with methanol and analyzed using the method presented in Section 2.5.

2.9. In vivo anesthetic pain relief evaluation

2.9.1. In vivo tail-flick test in rats

A tail-flick test was utilized to assess the *in vivo* analgesic effect (Zhang et al., 2017). A focused radiant heat source was applied as a harmful heat stimulus to the back surface of the tail. LID loaded NLC, free LID (concentration of LID was 2%), TAT/PB NLC, and 0.9% saline were smeared onto the tail surface for 5 min, separately. Then the tail-flick test started and lasted for a total of 75 min, with every 5 min for the first 30 min and every 15 min for the last 45 min. The maximum possible effect (MPE) was calculated to represent the analgesic effect e using formulation (3):

$$\text{MPE } (\%) = \frac{(\text{Latency after drug apply} - \text{Latency before drug apply})}{(\text{Latency of 10 s} - \text{Latency before drug apply})} \times 100.$$

Latency before and after the drug applies was determined by the average of the measurements post or before the drug administration. Ten seconds of cutoff latency was set to avoid tissue damage of rats.

2.9.2. In vivo analgesia duration test in mice

An electrical stimulation test was used to determine the analgesia duration of mice after sample application (Grant et al., 2000; Li et al., 2019). LID loaded NLC, free LID (concentration of LID was 2%), TAT/PB NLC, and 0.9% saline were injected subcutaneously into the abdomen of the mice. A current generator was used to measure the analgesic effect by the response of sound to electrical stimulation (increasing slowly from 1 to 8 mA) directly over the skin of the abdomen at the injection site and the analgesic effect was determined by the percentage of mice that generated vocal responses. 100% analgesia was confirmed by that one group of mice did not vocalize under the electric stimulation; 50% analgesia was achieved by half of the mice in the same group showed vocal responses; no analgesia was indicated by the whole group of mice made sounds when received electrical stimulation.

2.10. Statistical analysis

All the results were expressed as mean ± standard derivation. Comparisons were made using Student's *t*-tests or ANOVA. Statistical significance was set at $^*p < .05$.

3. Results

3.1. Characterization of PB-PEG-DSPE

PB-PEG-DSPE was characterized by ^{1}H NMR. ^{1}H NMR (300 MHz, $CDCl_3$) spectrum (Figure 1): δ 0.95 (–CH_3 of DSPE), 1.29 (–CH_2– of DSPE), 2.18 (–CH_2– of –NHCOCH_2–), 3.21 (–CH_2– of –NHCH_2–), 3.66 (–CH_2–C–O– of PEG), 4.02 (–CH_2– of –CH_2CONH–), 4.33 (–CH_2– of –O–CH_2–CONH–), 7.68–8.12

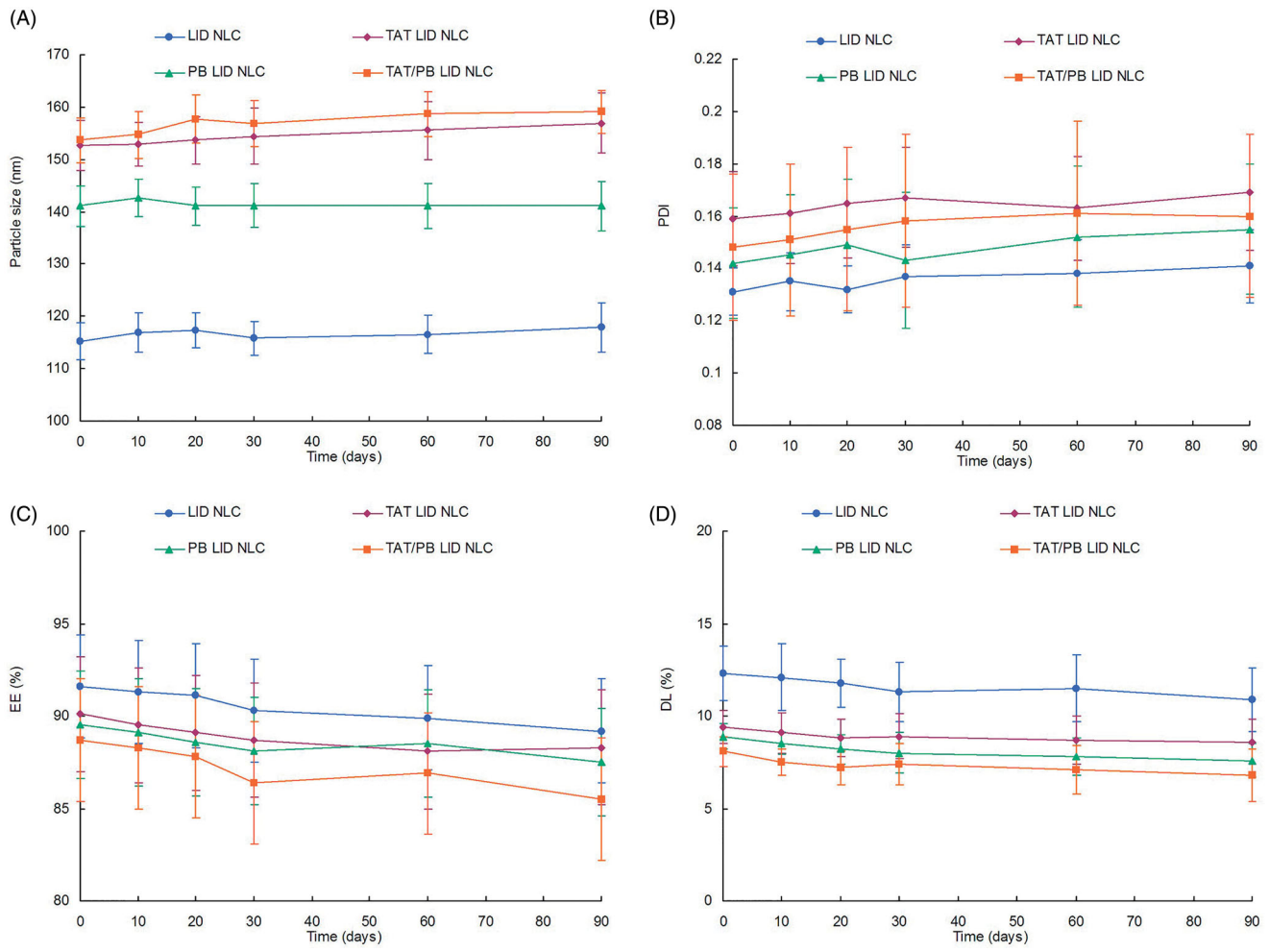

Figure 3. Storage stability of NLC. The NLC showed no significant change on size (A), PDI (B), EE (C), and DL (D) during the storage at 2–8 °C for a period of 90 days. Data presented as mean ± standard derivation ($n = 6$).

(–CH– of PB). These peaks demonstrated the formation of PB-PEG-DSPE.

3.2. Characterization of NLC

The transmission electron microscope image revealed that TAT/PB LID NLC have a spherical structure with some coats over the particles. The size of NLC was about 100 nm with moderately polydispersed particle size distribution. The size of TAT/PB LID NLC tested by DLS was 153.6 ± 4.3 nm (Table 1). However, undecorated LID NLC had a size of 115.3 ± 3.6 nm. The PDI values of NLC vary from 0.13 ± 0.01 to 0.16 ± 0.03. Zeta potentials of NLC were negative, between −20.7 and −29.3 mV. EE of LID loaded NLC was around 90%, corresponding to the DL of 8.1 ± 1.7 to 12.3 ± 1.5%. The NLC showed no significant change in size, PDI, EE, and DL during the storage at 2–8 °C for a period of 90 days (Figure 3).

3.3. In vitro LID release of NLC

Release profiles of kinds of NLC formulations were different (Figure 4). The drug release of LID NLC was the fastest; over 80% of LID was released from NLC at the time point of 24 h. On the contrary, LID was released at a much slower rate on other decorated NLC, taking over 36 h to complete the release procedure. The slowest release rates were observed on TAT LID NLC, which could be evidence of the existence of TAT molecule in the surface of particles may introduce a more sustained release to the system.

3.4. In vitro percutaneous penetration effect of NLC

Cumulative LID permeation profiles of LID loaded NLC was different from free LID (Figure 5). Free LID showed direct permeation during the first 2 h and then did not penetrate for the rest of the time. On the other hand, LID loaded NLC showed sustained and continuous penetration effects. At 72 h of study, TAT/PB LID NLC (851.2 ± 25.3 μg/cm^2) showed remarkably better percutaneous penetration ability than PB LID NLC (610.7 ± 22.1 μg/cm^2) and TAT LID NLC (551.9 ± 21.8 μg/cm^2) ($p < .05$). TAT LID NLC also permeated more amount of LID compared with non-modified LID NLC (428.2 ± 21.4 μg/cm^2) ($p < .05$).

3.5. In vivo anesthetic pain relief in rats

Tail-flick test revealed that blank TAT/PB NLC without LID exhibited no analgesic efficiency (Figure 6). Free LID

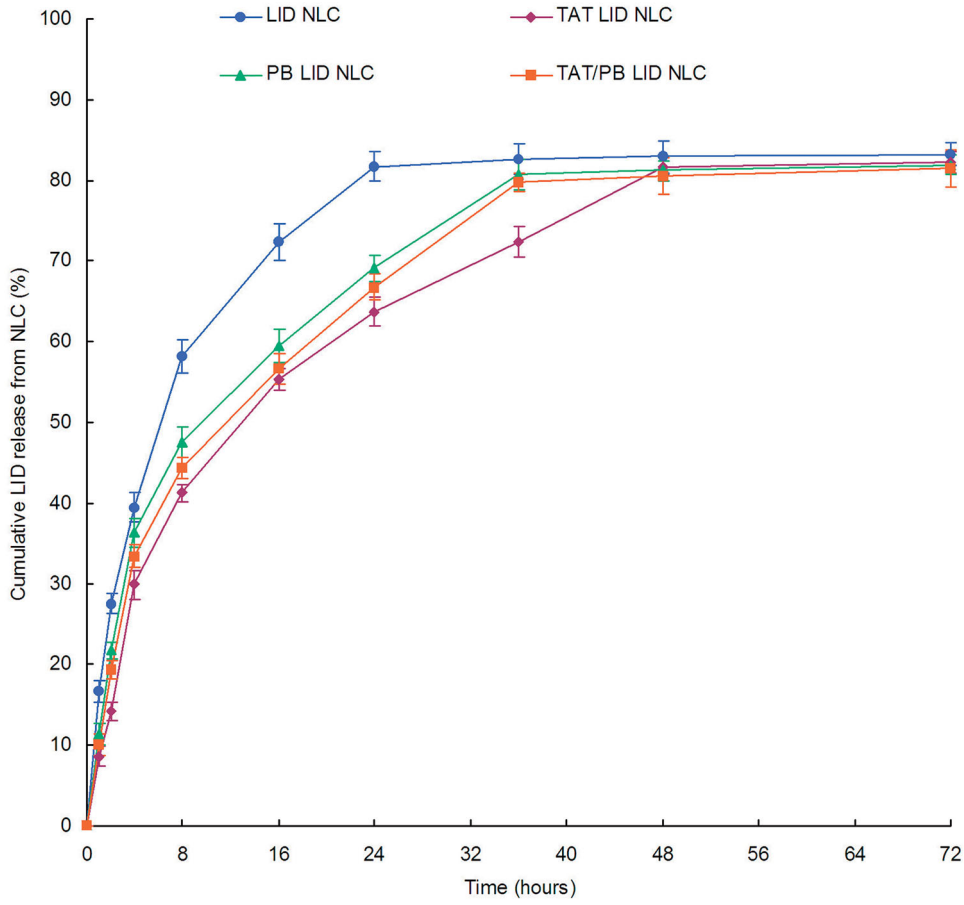

Figure 4. *In vitro* drug release profiles of NLC. Dialysis method was applied to evaluate the *in vitro* drug release of LID from the NLC. Data presented as mean ± standard derivation ($n = 6$).

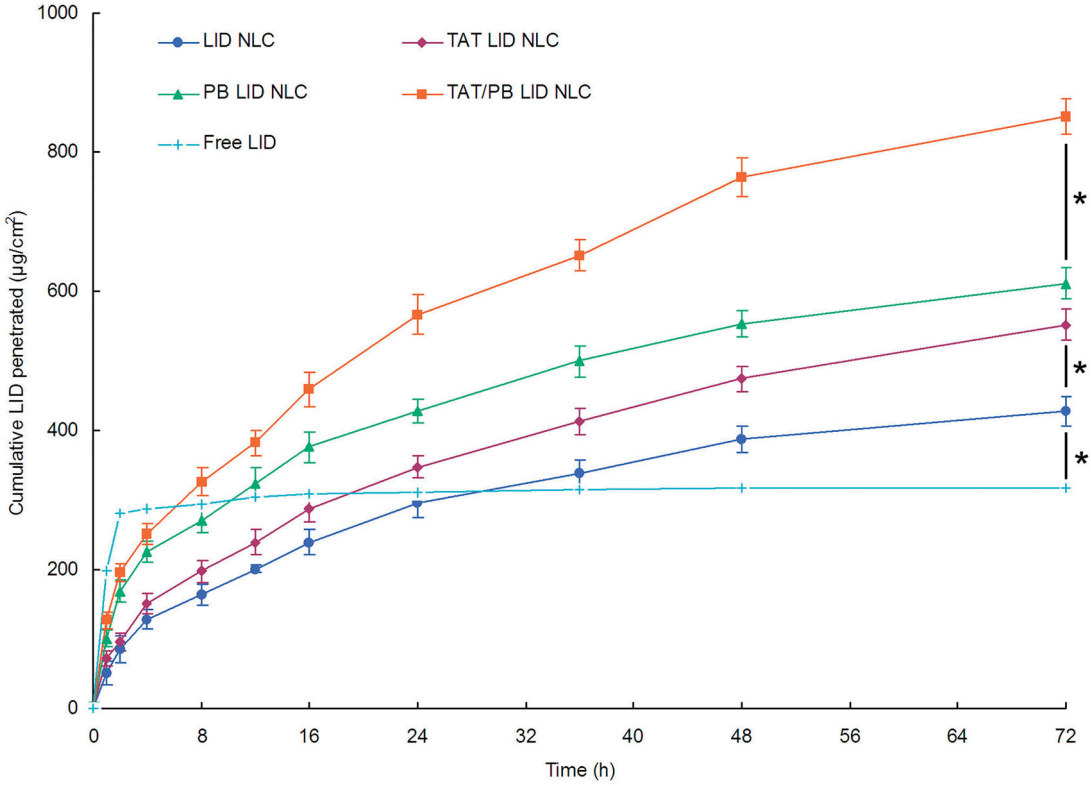

Figure 5. *In vitro* percutaneous penetration effect of NLC. *In vitro* skin permeation study was carried out in Vertical Franz-type diffusion cells with cross-sectional area of 5.93 cm^2 and 7.0 mL cell volume. Data presented as mean ± standard derivation ($n = 6$). $^*p < .05$.

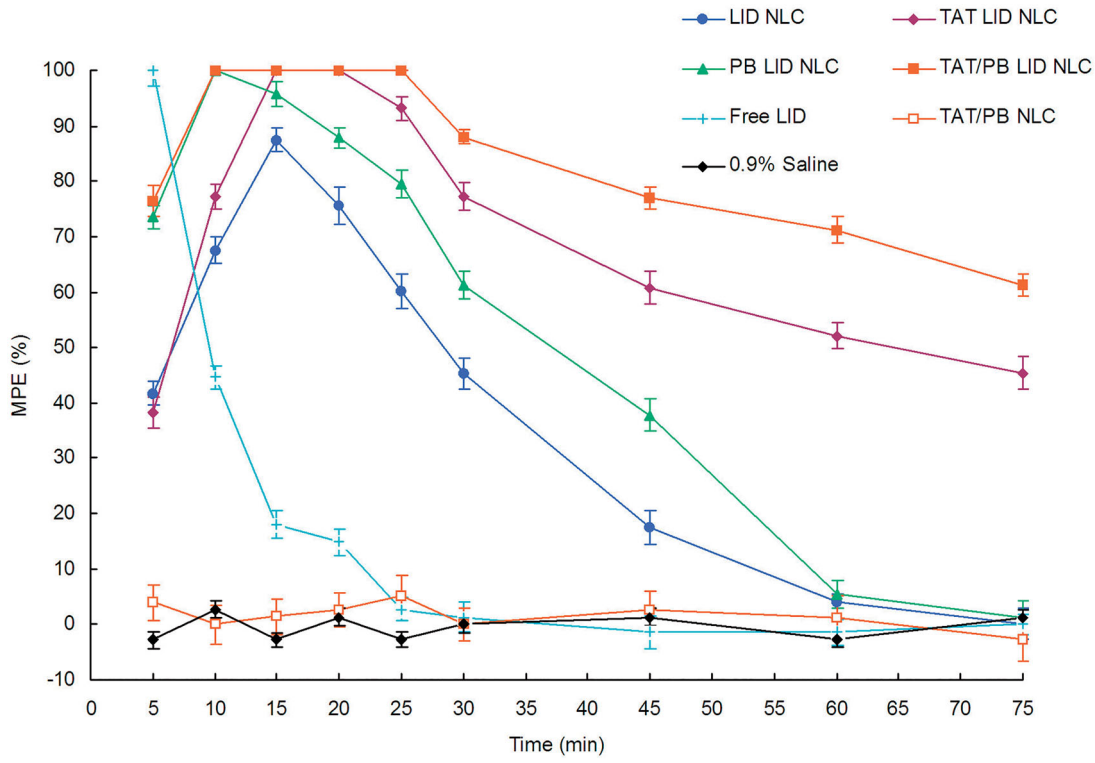

Figure 6. *In vivo* anesthetic pain relief effect was assessed by the tail-flick test in rats. A harmful heat stimulus was applied to the back surface of the tail by a focused radiant heat source. Percentage of the maximum possible effect (MPE) was applied to express the anesthetic pain relief effect. Data presented as mean-±standard derivation ($n = 8$).

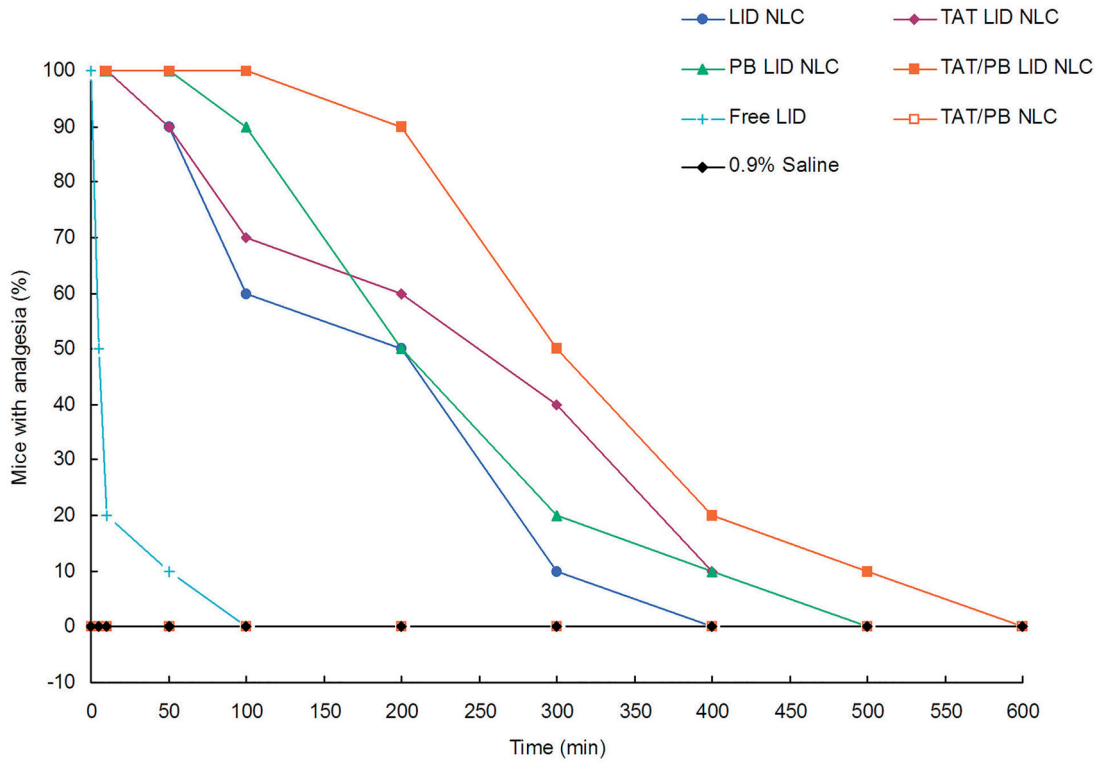

Figure 7. *In vivo* analgesia duration test was applied by electrical stimulation testing in mice. A current generator was used to measure the analgesic effect by the vocal response to electrical stimulation (starting at 1 mA and increasing to a maximum of 8 mA) directly over the skin of the abdomen at the injection site.

illustrated an effective but temporary analgesic effect, which quickly declined in the first 15 min. Longer anesthetic pain relief effects were observed on LID loaded NLC formulations when compared with free LID. TAT/PB LID NLC exhibited the most prominent anesthetic effect than single ligand decorated or undecorated LID NLC, with the highest and the most durable anesthetic analgesic effect *in vivo*.

3.6. In vivo analgesia duration in mice

Analgesic results in mice indicated a significantly prolonged analgesia effect of LID NLC compared with free LID (Figure 7). TAT/PB LID NLC showed the longest and best analgesia efficiency than other formulations, which are in accordance with the *in vivo* analgesic results in rats. Blank TAT/PB NLC illustrated no analgesia ability and the profile was in line with the 0.9% saline control group.

4. Discussion

The overall aim of this study was to achieve a strong and prolonged analgesia effect by using TAT and PB multi-decorated, LID loaded NLC. The size of NLC was about 100 nm in TEM and 153.6 ± 4.3 nm tested by DLS. The size determined by TEM is smaller than DLS. This phenomenon can be explained by the difference between DLS and TEM. DLS used the Stokes–Einstein equation to provide the statistical average hydrodynamic size of the particles based on the diffusion coefficient of the particles in the liquid phase, while TEM provided the estimation of the projected area diameter of the particles in the dry state under high vacuum (Ito et al., 2004). After decorated with TAT and PB, the size of LID NLC increased from 115.3 to 153.6 nm (TAT/PB LID NLC), which means the ligands on the surface enlarged the particle size. However, similar sizes were obtained by TAT/PB LID NLC and blank TAT/PB NLC, which could be evidence that drug loading does not change the diameter of the NLC.

In many practical applications, the stability of colloids is an important issue in colloid-based technology and formulation (Loza et al., 2019). The thermodynamic stability of particles is lower due to the large specific surface area, compared with the system with large particles. The free surface energy is higher and they tend to be agglomerated with the passage of time. The deposition, diffusion, and agglomeration of particles are related to the size, density, and surface properties of particles, and have a great influence on the concept of dose-response. The NLC showed no significant change in size, PDI, EE, and DL during the storage at 2–8 °C for a period of 90 days, which means the NLC was stable.

The release of LID was significantly prolonged by the NLC systems in different content. The sustained release of LID from NLC may be related to the diffusion of LID from NLC and the degradation or hydrolysis of NLC (Danafar et al., 2014). After decoration, LID was released at a much slower rate from NLC, which could prove the existence of ligands in the surface of particles may introduce a slower release behavior. NLC has been widely used to prolong the release of drugs and achieve long-lasting efficiency (Zhang et al., 2014; Cao et al., 2019). PEGylated nanoparticles were also determined to sustain the release rates of the drug delivery systems (Huang et al., 2017). In this study, PEGylated NLC could guarantee the permeation and sustained release of the anesthetic and achieve long-lasting anesthesia.

In vitro permeation profiles showed that LID loaded NLC showed more sustained and continuous penetration effects compared with free LID. At 72 h of study, TAT/PB LID NLC showed remarkably better percutaneous penetration ability than PB LID NLC and TAT LID NLC, this may be due to the combined effect of PB and TAT. PB has been described as an effective permeation enhancer and may have an influence on the skin permeation of LID NLC (Mathew & Kuriakose, 2013). The transdermal property of PB decorated TAT/PB LID NLC and PB LID NLC is significantly improved compared with LID NLC, indicating that it has good transdermal property. NLCs have a natural affinity for skin lipids. This feature enables them to facilitate drug transport and facilitates drug entry from carriers into the skin zone (Vitorino et al., 2013). LID NLC showed better penetration ability than free LID, which may be attributed to the character of NLC.

Two different experiments (in rats and mice) were applied to evaluate the *in vivo* analgesic efficacy of NLC formulations. TAT/PB LID NLC exhibited the most prominent anesthetic effect than single ligand decorated or undecorated LID NLC, with the longest and best analgesia efficiency *in vivo*. NLC formulations showed prolonged analgesia than free LID, which makes the NLC system a feasible and attractive option (Cohen et al., 2012). It is widely used to transfer bioactive compounds across cell membranes by fuzing with the cell-penetrating peptides (CPPs) (such as TAT) (Nagahara et al., 1998). Current researches have also shown that PB increases the ability of CPPs to enter cells through lipid bilayer (Takeuchi et al., 2006; Candan et al., 2012). According to the *in vitro* and *in vivo* results, the resulting TAT/PB LID NLC exhibited good skin penetration and anesthetic pain relief efficiency, which could be applied as a promising anesthesia system.

5. Conclusion

In summary, a novel PB (PB-PEG-DSPE) compound was synthesized by the amide action of the carboxylic acid group of PB with the amido groups of DSPE-PEG. TAT and PB multi-decorated TAT/PB LID NLC exhibited good skin penetration and anesthetic efficiency, which can be applied as a promising anesthesia system.

Disclosure statement

No potential conflict of interest was reported by the author(s).

Funding

The work was financially supported by the Shandong Medical and Health Science and Technology Development project (2017WS176).

References

Candan G, Michiue H, Ishikawa S, et al. (2012). Combining poly-arginine with the hydrophobic counter-anion 4-(1-pyrenyl)-butyric acid for protein transduction in transdermal delivery. Biomaterials 33:6468–75.

Cao C, Wang Q, Liu Y. (2019). Lung cancer combination therapy: doxorubicin and β-elemene co-loaded, pH-sensitive nanostructured lipid carriers. Drug Des Devel Ther 13:1087–98.

Chen C, You P. (2017). A novel local anesthetic system: transcriptional transactivator peptide-decorated nanocarriers for skin delivery of ropivacaine. Drug Des Devel Ther 11:1941–9.

Cohen R, Kanaan H, Grant GJ, Barenholz Y. (2012). Prolonged analgesia from Bupisome and Bupigel formulations: from design and fabrication to improved stability. J Control Release 160:346–52.

Danafar H, Davaran S, Rostamizadeh K, et al. (2014). Biodegradable m-PEG/PCL core-shell micelles: preparation and characterization as a sustained release formulation for curcumin. Adv Pharm Bull 4:501–10.

de Araújo DR, da Silva DC, Barbosa RM, et al. (2013). Strategies for delivering local anesthetics to the skin: focus on liposomes, solid lipid nanoparticles, hydrogels and patches. Expert Opin Drug Deliv 10: 1551–63.

Franz-Montan M, Ranali J, Ramacciato JC, et al. (2008). Ulceration of gingival mucosa after topical application of EMLA: report of four cases. Br Dent J 204:133–4.

Franz-Montan M, Ribeiro LNM, Volpato MC, et al. (2017). Recent advances and perspectives in topical oral anesthesia. Expert Opin Drug Deliv 14:673–84.

Grant GJ, Piskoun B, Lin A, Bansinath M. (2000). An in vivo method for the quantitative evaluation of local anesthetics. J Pharmacol Toxicol Methods 43:69–72.

Gul R, Ahmed N, Shah KU, Khan GM. (2018). Functionalised nanostructures for transdermal delivery of drug cargos. J Drug Target 26: 110–22.

Huang X, Huang J, Leng D, et al. (2017). Gefitinib-loaded DSPE-PEG2000 nanomicelles with CD133 aptamers target lung cancer stem cells. World J Surg Oncol 15:167.

Ito T, Sun L, Bevan MA, Crooks RM. (2004). Comparison of nanoparticle size and electrophoretic mobility measurements using a carbon-nanotube-based coulter counter, dynamic light scattering, transmission electron microscopy, and phase analysis light scattering. Langmuir 20: 6940–5.

Karande P, Jain A, Ergun K, et al. (2005). Design principles of chemical penetration enhancers for transdermal drug delivery. Proc Natl Acad Sci USA 102:4688–93.

Karande P, Jain A, Mitragotri S. (2004). Discovery of transdermal penetration enhancers by high-throughput screening. Nat Biotechnol 22: 192–7.

Kumar S, Zakrewsky M, Chen M, et al. (2015). Peptides as skin penetration enhancers: mechanisms of action. J Control Release 199:168–78.

Li A, Yang F, Xin J, Bai X. (2019). An efficient and long-acting local anesthetic: ropivacaine-loaded lipid-polymer hybrid nanoparticles for the control of pain. Int J Nanomedicine 14:913–20.

Loza K, Epple M, Maskos M. (2019). Stability of nanoparticle dispersions and particle agglomeration. In Gehr P, Zellner R, eds. Biological responses to nanoscale particles. NanoScience and technology. Cham (Switzerland): Springer, 85–100.

Mandal B, Mittal NK, Balabathula P, et al. (2016). Development and in vitro evaluation of core-shell type lipid-polymer hybrid nanoparticles for the delivery of erlotinib in non-small cell lung cancer. Eur J Pharm Sci 81:162–71.

Mathew TV, Kuriakose S. (2013). 4-(1-Pyrenyl)butyric acid-functionalised chitosan as a matrix for AgNP: photoresponsive and thermal properties. J Polym Res 20:1–8.

Mueller J, Oliveira JSL, Barker R, et al. (2016). The effect of urea and taurine as hydrophilic penetration enhancers on stratum corneum lipid models. Biochim Biophys Acta 1858:2006–18.

Müller RH, Shegokar R, Keck CM. (2011). 20 years of lipid nanoparticles (SLN and NLC): present state of development and industrial applications. Curr Drug Discov Technol 8:207–27.

Münch S, Wohlrab J, Neubert RHH. (2017). Dermal and transdermal delivery of pharmaceutically relevant macromolecules. Eur J Pharm Biopharm 119:235–42.

Nagahara H, Vocero-Akbani AM, Snyder EL, et al. (1998). Transduction of full-length TAT fusion proteins into mammalian cells: TAT-p27Kip1 induces cell migration. Nat Med 4:1449–52.

Nasrollahi SA, Taghibiglou C, Azizi E, Farboud ES. (2012). Cell-penetrating peptides as a novel transdermal drug delivery system. Chem Biol Drug Des 80:639–46.

Ookubo N, Michiue H, Kitamatsu M, et al. (2014). The transdermal inhibition of melanogenesis by a cell-membrane-permeable peptide delivery system based on poly-arginine. Biomaterials 35:4508–16.

Patlolla RR, Desai PR, Belay K, Singh MS. (2010). Translocation of cell penetrating peptide engrafted nanoparticles across skin layers. Biomaterials 31:5598–607.

Pham QD, Björklund S, Engblom J, et al. (2016). Chemical penetration enhancers in stratum corneum - relation between molecular effects and barrier function. J Control Release 232:175–87.

Pino CJ, Scherer MA, Shastri VP. (2014). Investigation of the transdermal transport of charged local anesthetics in the presence of triterpene saponin glycosides. Drug Deliv Transl Res 4:131–8.

Song Y, Cai H, Yin T, et al. (2018). Paclitaxel-loaded redox-sensitive nanoparticles based on hyaluronic acid-vitamin E succinate conjugates for improved lung cancer treatment. Int J Nanomedicine 13:1585–600.

Takeuchi T, Kosuge M, Tadokoro A, et al. (2006). Direct and rapid cytosolic delivery using cell-penetrating peptides mediated by pyrenebutyrate. ACS Chem Biol 1:299–303.

Vitorino C, Almeida J, Gonçalves LM, et al. (2013). Co-encapsulating nanostructured lipid carriers for transdermal application: from experimental design to the molecular detail. J Control Release 167:301–14.

Wang Y, Su W, Li Q, et al. (2013). Preparation and evaluation of lidocaine hydrochloride-loaded TAT-conjugated polymeric liposomes for transdermal delivery. Int J Pharm 441:748–56.

Wang Y, Wang S, Shi P. (2016). Transcriptional transactivator peptide modified lidocaine-loaded nanoparticulate drug delivery system for topical anesthetic therapy. Drug Deliv 23:3193–9.

Williams AC, Barry BW. (2004). Penetration enhancers. Adv Drug Deliv Rev 56:603–18.

You P, Yuan R, Chen C. (2017). Design and evaluation of lidocaine- and prilocaine-coloaded nanoparticulate drug delivery systems for topical anesthetic analgesic therapy: a comparison between solid lipid nanoparticles and nanostructured lipid carriers. Drug Des Devel Ther 11: 2743–52.

Yue Y, Zhao D, Yin Q. (2018). Hyaluronic acid modified nanostructured lipid carriers for transdermal bupivacaine delivery: in vitro and in vivo anesthesia evaluation. Biomed Pharmacother 98:813–20.

Zhang C, Peng F, Liu W, et al. (2014). Nanostructured lipid carriers as a novel oral delivery system for triptolide: induced changes in pharmacokinetics profile associated with reduced toxicity in male rats. Int J Nanomedicine 9:1049–63.

Zhang Y, Yue Y, Chang M. (2017). Local anaesthetic pain relief therapy: in vitro and in vivo evaluation of a nanotechnological formulation coloaded with ropivacaine and dexamethasone. Biomed Pharmacother 96:443–9.

Zhao X, Sun Y, Li Z. (2018). Topical anesthesia therapy using lidocaine-loaded nanostructured lipid carriers: tocopheryl polyethylene glycol 1000 succinate-modified transdermal delivery system. Drug Des Devel Ther 12:4231–40.